THE GEOLOGICAL RECORD OF METEORITE IMPACTS

Gordon R. Osinski

Canadian Space Agency, 6767 Route de l'Aeroport, St-Hubert, QC J3Y 8Y9 Canada,
Email: gordon.osinski@space.gc.ca

ABSTRACT

Meteorite impact structures are found on all planetary bodies in the Solar System with a solid surface. On the Moon, Mercury, and much of Mars, impact craters are the dominant landform. On Earth, 174 impact sites have been recognized, with several more new craters being discovered each year. The terrestrial impact cratering record is critical for our understanding of impacts as it currently provides the only ground-truth data on which to base interpretations of the cratering record of other planets and moons. In this contribution, I summarize the processes and products of impact cratering and provide and an up-to-date assessment of the geological record of meteorite impacts.

1. INTRODUCTION

It is now widely recognized that impact cratering is a ubiquitous geological process that affects all planetary objects with a solid surface (e.g., [1]). One only has to look up on a clear night to see that impact structures are the dominant landform on the Moon. The same can be said of all the rocky and icy bodies in the solar system that have retained portions of their earliest crust. On Earth, however, erosion, volcanic resurfacing, and tectonic activity are continually erasing impact craters from the rock record. Despite this, 174 confirmed impact structures have been documented to date with several more 'new' sites being recognized each year (Fig. 1) [2].

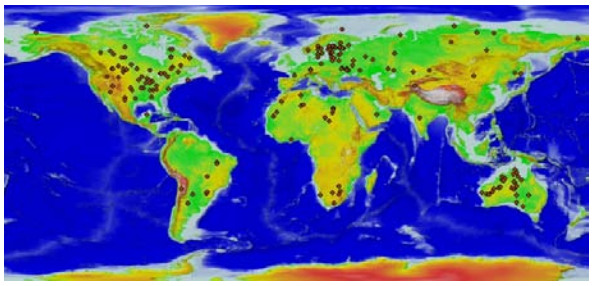

Fig. 1. Location of the 174 recognized terrestrial impact structures superimposed on a digital elevation map of the Earth. Location of structures from the Earth Impact Database [2] (see Appendix 1).

2. FORMATION OF METEORITE IMPACT STRUCTURES

The formation of hypervelocity impact craters has been divided, somewhat arbitrarily, into three main stages [3] (Fig. 2): (1) contact and compression, (2) excavation, and (3) modification. A further stage of "hydrothermal and chemical alteration" is also considered as a separate, final stage in the cratering process (e.g., [4]), and is also described below.

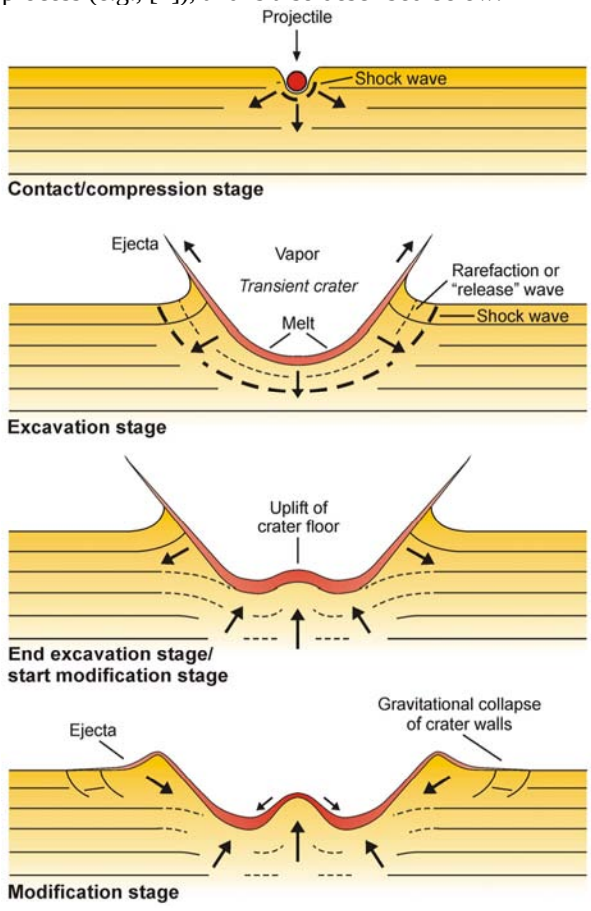

Fig. 2. Series of schematic cross sections depicting the formation of a terrestrial complex impact structure (i.e., diameter >2–4 km). From [5].

2.1. Contact and compression

The first stage of an impact event begins when the projectile, either an asteroid or comet, contacts the surface of the target (Fig. 2). The projectile penetrates no more than 1–2 times its diameter [4], before transferring its kinetic energy into the target in the form of shock waves that are created at the boundary between the compressed and uncompressed target material [6]. These shock waves subsequently propagate both into the target sequence and back into the projectile itself. When the reflected shock wave reaches the 'free' upper surface of the projectile, it is reflected back into the projectile as a rarefaction, or tensional wave [7]. The passage of this rarefaction wave through the projectile causes it to unload from high shock pressures, resulting in the complete melting and/or vaporization of the projectile itself [3, 6]. The increase in internal energy accompanying compression and subsequent rarefaction results in the virtually instantaneous melting and/or vaporization of a volume of target material close to the point of impact, producing characteristic impact melt rocks and glass-bearing breccias that form the crater-fill impactites in many terrestrial impact craters [7, 8].

For impact craters formed in crystalline targets, these crater-fill impact melt rocks display characteristic igneous textures and features (e.g., columnar jointing; Fig. 3). In contract, the crater-fill impactites in craters developed in sedimentary or mixed crystalline–sedimentary targets, do not display such obvious characteristics (e.g., Fig. 4), which has led to many uncertainties regarding the importance of impact melting in volatile-rich sedimentary target rocks [5]. However, recent work has shown that impact melting is an important process during impacts into sedimentary targets [9-12] (Fig. 4).

Fig. 3. Impact melt rocks at the ~28 km diameter, ~36 Ma Mistastin impact structure, Canada. Notice the well-developed columnar jointing on the ~80 m high cliff face. Photo courtesy of D. Wilton.

Fig. 4. Crater-fill impactites at the Haughton impact structure, Canada, interpreted as carbonate-rich impact melt breccias [12].

The point at which the projectile is completely unloaded is generally taken as the end of the contact and compression stage [6]. The duration of this initial stage depends on the projectile's size, composition, and impact velocity; however, it lasts no more than a few seconds for all but the largest basin-forming impacts [6].

2.2. Excavation stage

The transition from the initial contact and compression stage, into the excavation stage is a continuum. It is during this stage that the actual impact crater is opened up by complex interactions between the expanding shock wave and the original ground surface [6]. During the excavation stage, the roughly hemispherical shock wave propagates out into the target sequence (Fig. 2). This causes target material to be set in motion, with an outward radial trajectory. At the same time, shock waves that initially travelled upwards intersect the ground surface and generate rarefaction waves that propagate back downwards into the target sequence [6]. The combination of the outward-directed shock waves and the downward-directed rarefaction waves produces an 'excavation flow' and generates a so-called 'transient cavity' (Figs. 2, 3) [13, 14]. The different trajectories of material in different regions of the excavation flow field result in the partitioning of the transient cavity into an upper 'excavated zone' and a lower 'displaced zone' (Fig. 5). Material in the excavated zone is ejected beyond the transient cavity rim, while material in the displaced zone remains within the transient cavity [15]. It is notable that the excavation flow lines transect the hemispherical pressure contours, so that ejecta will contain material from a range of different shock levels, including shock-melted target lithologies.

A portion of the melt and rock debris that originates beneath the point of impact remains in the transient cavity [8]. This material forms the crater-fill impactites in terrestrial impact craters (Figs. 3, 4). Eventually, a point is reached at which the shock and rarefaction waves can no longer excavate or displace

target rock and melt [16]. At the end of the excavation stage, a mixture of melt and rock debris forms a lining to the transient cavity. Calculations suggest that the excavation stage for a 200 km diameter crater requires ~90 s [6].

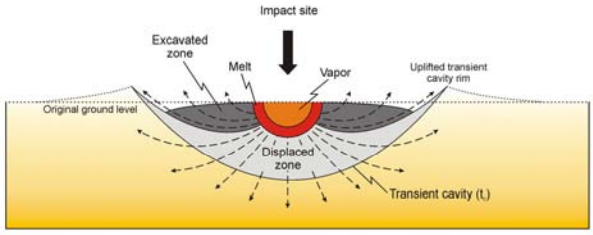

Fig. 5. Theoretical cross section through a transient cavity showing the locations of impact metamorphosed target lithologies. Excavation flow lines (dashed lines) open up the crater and result in excavation of material from the upper one-third to one-half the depth of the transient cavity. Modified after Grieve [17] and Melosh [6].

2.3. Modification stage

The effects of the modification stage are governed by the size of the transient cavity and the properties of the target rock lithologies [18]. For crater diameters <2–4 km on Earth, the transient cavity undergoes only minor modification resulting in the formation of a simple bowl-shaped crater (Figs. 6a, 7). However, above a certain size threshold (generally quoted as >2–4 km diameter on Earth, but see discussion in section 3), the transient cavity is unstable and undergoes modification by gravitational forces, producing a so-called complex impact crater (Figs. 2, 6b,c, 8) [19]. Uplift of the transient crater floor occurs leading to the development of a central uplift (Figs. 2, 6b). Subsequently, the initially steep walls of the transient crater collapse under gravitational forces (Fig. 2). Numerical models suggest that the maximum depth of the transient cavity is attained before the maximum diameter is reached (e.g., [20]). Thus, uplift of the crater floor may commence before the maximum diameter has been reached. As French [16] notes, the modification stage has no clearly marked end. Processes that are intimately related to complex crater formation, such as the uplift of the crater floor and collapse of the walls, merge into normal geological processes such as mass movement, erosion, etc.

2.4. Post-impact hydrothermal activity

Impact events generate pressures and temperatures that can melt and/or heat substantial volumes of target material. Interaction of these hot rocks with groundwaters and surface water can lead to the development of an impact-generated hydrothermal system [21]. Recent studies suggest that impact-induced hydrothermal activity will occur following the majority of impact events, with some exceptions for small craters or those formed in arid environments [22, 23]. The circulation of hydrothermal fluids through impact craters can lead to substantial alteration and mineralization of impactites and target rocks. Thus, the recognition of impact-associated hydrothermal deposits is important in understanding the evolution of impact craters through time.

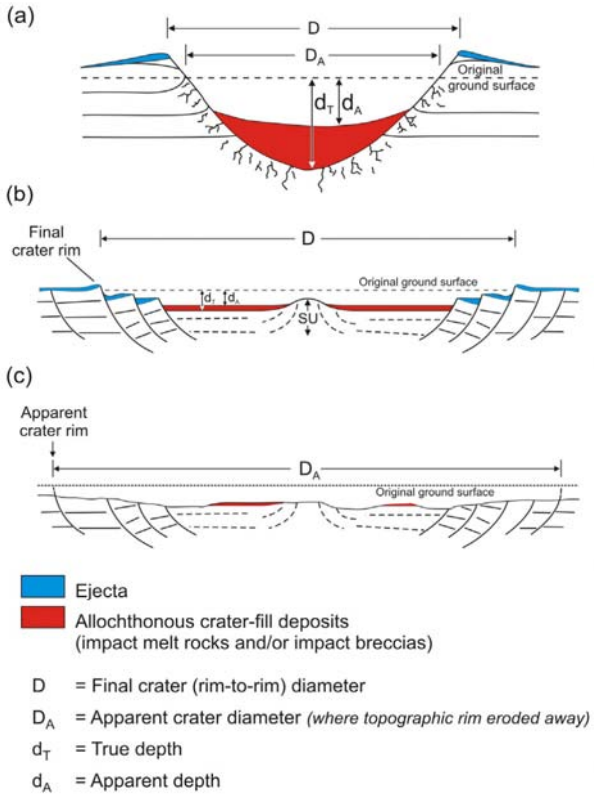

Fig. 6. Series of schematic cross sections through a simple (a) and complex (b, c) impact structure. This figure also illustrates the various diameters and depths associated with hypervelocity impact craters (see Turtle et al. [24] for a detailed review and discussion of the different connotations associated with "crater diameter"). It is important to note that for the majority of terrestrial impact structures, which are eroded, the apparent crater diameter (D_A) will be the only value obtainable. This is not the same metric quoted in numerical modeling studies, where the final crater (rim-to-rim) diameter (D) is typically used. Modified after Turtle et al. [24].

3. MORPHOLOGY OF IMPACT CRATERS

Impact craters are subdivided into two main groups based on morphology: simple and complex. Simple craters comprise a bowl-shaped depression that is similar in shape to the initial transient cavity (Figs. 6a, 7). Complex impact structures generally have a structurally complicated rim, a down-faulted annular trough, and an uplifted central area (Fig. 6b). These features form as a result of gravitational adjustments of the initial crater during the modification stage of impact crater formation (see section 2.3).

Fig. 7. Oblique aerial view of the 1.2 km diameter Meteor Crater, Arizona. Photo courtesy of T. Bunch.

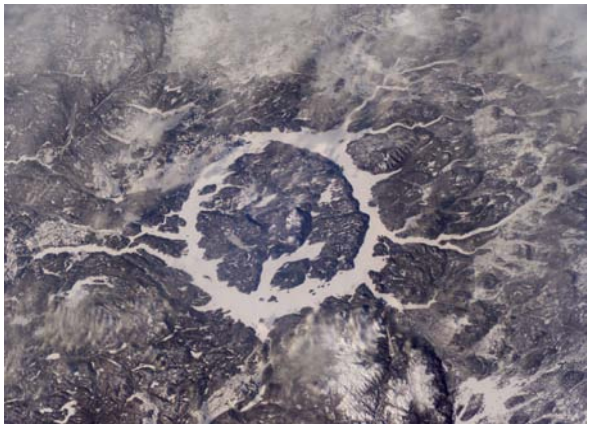

Fig. 8. View from the Space Shuttle of the ~100 km diameter Manicouagan impact structure, Canada. Image courtesy of Earth Sciences and Image Analysis Laboratory, NASA Johnson Space Center. ISS012 Roll: E Frame: 15880.

It is widely cited that the transition from simple to complex craters on Earth occurs at a smaller diameter in sedimentary (2 km) as opposed to crystalline targets (4 km). This dates back to the work of Dence [25] who based this observation on a compilation of the 50 known impact structures at that time. Figure 9 shows that this inference may require updating, given the current impact cratering record. In particular, it is apparent that the simple-to-complex transition for craters developed in crystalline and mixed sedimentary-crystalline targets occurs over a range of diameters (~3–4 km). For sedimentary targets, the average transition diameter does appear to be at a slightly lower value of ~3 km, but the difference between craters developed in different target rocks is not as pronounced as previously noted. In addition, there is also the notable exception of the ~5 km diameter Goat Paddock impact structure, Australia, which appears to be a simple crater but with features transitional to the complex morphology [26]. It should be noted that Figure 8 was compiled using those craters where the diameter was deemed reliable by the author. However, this relies on the accurateness of the literature. In addition, there are also complications due to differing erosion levels and differences in opinion as to what crater diameter actually means (e.g., apparent versus final crater diameter; Fig. 6), which is often not clear in the literature (see Turtle [24] for a review).

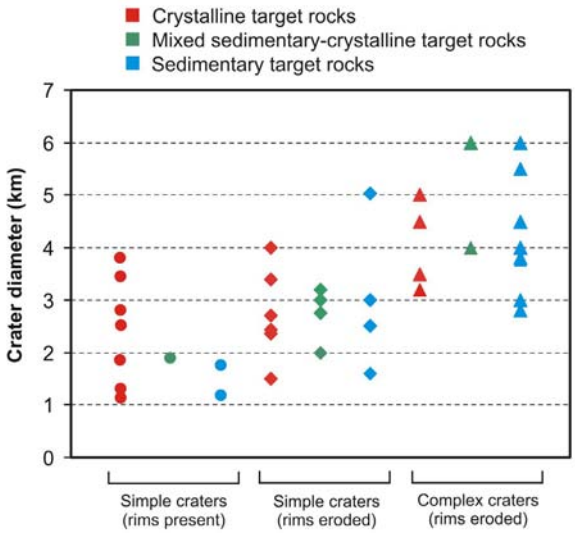

Fig. 9. Classification of all known impact structures 1–6 km in diameter with reliable metrics.

4. IMPACT CRATERING v. ENDOGENOUS GEOLOGICAL PROCESSES

Meteorite impact events differ in several ways from more familiar endogenous geological processes such as earthquakes and volcanic eruptions. In the past, there has been much confusion and controversy surrounding impacts, in part, due to their rarity, even over geological timescales. Unlike large earthquakes, volcanic explosions, or tsunamis, there have been no historical examples of crater-forming impact events

[16]. Major differences between impact events and other geological processes include: (1) the extreme physical conditions (Fig. 10); (2) the concentrated nature of the energy release at a single point on the Earth's surface; (3) the virtually instantaneous nature of the impact process; and (4) the high strain rates involved (~104 s–1 to 106 s–1 for impacts versus 10–3 s–1 to 10–6 s–1 for endogenous tectonic and metamorphic processes) [16]. Impact events are, therefore, unlike any other geological process.

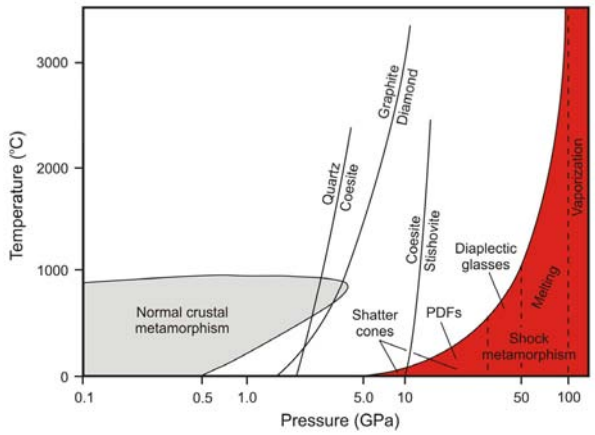

Fig. 10. Pressure–temperature (P–T) plot showing comparative conditions for shock metamorphism and 'normal' crustal metamorphism. The approximate P–T conditions needed to produce specific shock effects are indicated by vertical dashed lines below the exponential curve that encompasses the field of shock metamorphism. Modified from French [16].

5. THE RECOGNITION OF METEORITE IMPACT STRUCTURES

Several criteria may be used to identify hypervelocity impact structures, including the presence of a crater form and/or unusual rocks, such as breccias, melt rocks, and pseudotachylyte; however, on their own, these indicators do not provide definitive evidence for a meteorite impact structure. The general consensus within the impact community is that unequivocal evidence for hypervelocity impact takes the form of shock metamorphic indicators, either megascopic (e.g., shatter cones Fig. 11) or microscopic (e.g., planar deformation features, Fig. 12; diaplectic glass, Fig. 13), and the presence of high-pressure polymorphs (e.g., coesite, stishovite). Unfortunately, this requires investigation and preservation of suitable rocks within a suspected structure. However, this is often not possible for eroded and/or buried structures and/or structures presently in the marine environment (e.g., the Eltanin structure in the South Pacific), even though there is strong evidence for an impact origin.

A prime example is the controversy surrounding the Silverpit structure in the North Sea. Stewart and Allen [27] originally proposed that this structure was an impact crater based on high-resolution 3D seismic data and despite some opposition (e.g., [28]), most impact workers accept this; however, without drilling to retrieve samples, this structure is currently relegated to the list of "possible" impact structures. This is unfortunate as the seismic dataset for this structure surpasses that available for any known impact structure and may provide important insights into complex crater formation [27]. In order to try and address this issue, Stewart [29] proposed a framework for the identification of impact structures based on 3D seismic data, but this has received little attention to date within the impact community.

Fig. 11. Shatter cones developed in fine-grained limestones of the central uplift of the Haughton impact structure, Canada. The height of the image is 18 cm.

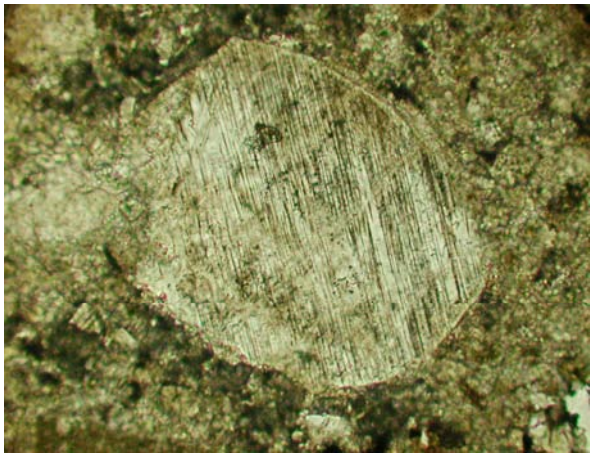

Fig. 12. Quartz grain displaying planar deformation features from the crater-fill impact melt breccias of the Haughton impact structure, Canada. Plane polarized light photomicrograph. Field of view is 2 mm.

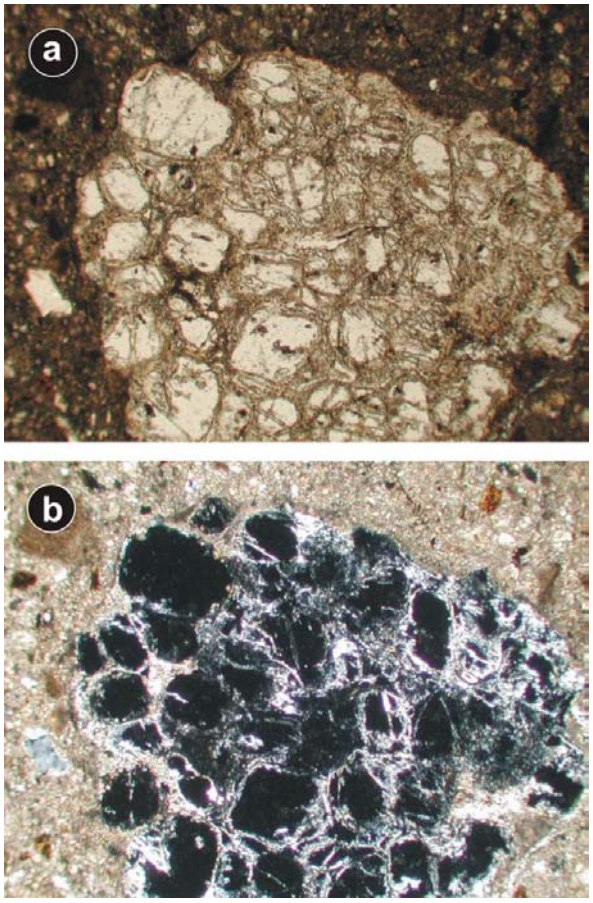

Fig. 13. Sandstone clast features from the crater-fill impact melt breccias of the Haughton impact structure, Canada. Comparison of Plane (a) and cross (b) polarized light photomicrographs reveals that the majority of the quartz grains have been transformed to diaplectic glass. Field of view is 4 mm.

6. THE TERRESTRIAL IMPACT CRATERING RECORD

It has been 100 years since D. Barringer published his landmark paper outlining the evidence for the impact origin of Meteor Crater, Arizona [30]. Since then, the inventory of known terrestrial impact structures has grown steadily through time (Fig. 14), with a current average detection rate of ~3–5 impact sites per year. Systematic field and remote sensing campaigns in Scandinavia [31] and Australia [32] have been particularly successful in the detection of new impact sites. Currently, there are 174 recognized terrestrial impact structures (Fig. 15) (i.e., structures where characteristic shock metamorphic criteria have been recognized) listed in the Earth Impact Database [2], hosted and updated by the University of New Brunswick, Canada.

Notwithstanding the problems surrounding the recognition of meteorite impact structures (see section 5), the potential for finding new impact sites and/or confirming suspected sites remains high, as exemplified by the recent compilation of Suspected Earth Impact Sites (SEIS) by D. Rajmon and published online at http://web.eps.utk.edu/ifsg.htm.

6.1. Spatial distribution of terrestrial impact structures

Despite the recognition of 174 terrestrial impact sites, the record is notably incomplete. There are still few impact sites in South America, Central Africa and large parts of Asia. Important questions remain as to whether this is due to the regional geology of these regions (e.g., lack of ancient, stable cratons), or if the scarcity of impact sites is due to a lack of detailed field and remote sensing studies and/or other factors, such as vegetation coverage or erosion.

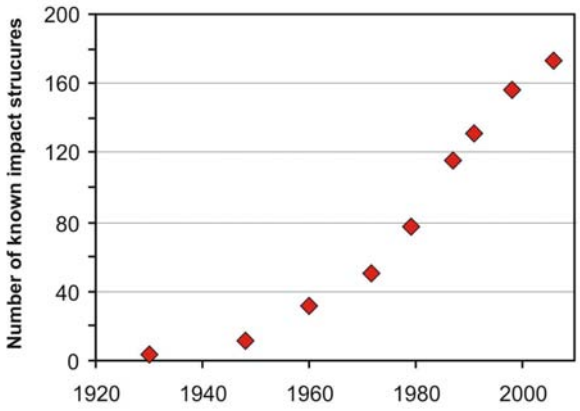

Fig. 14. Variation through time of the number of confirmed terrestrial impact structures. Note the increase in detection rate of impact structures in the 1970's, which is due to the recognition of shock metamorphic criteria (i.e., [33]).

6.2. Distribution of terrestrial impact structures with respect to target composition and setting

Figure 15 shows the distribution of impact structures with respect to the composition of the target rocks. Over two-thirds (96) of terrestrial craters formed, at least in part, in sedimentary target rocks. This is notable given the outstanding questions concerning the processes and products of impacts into volatile-rich, porous, layered sedimentary rocks (e.g., see the discussion in section 2.1 regarding impact melting in sedimentary target rocks).

The majority of the recognized impact sites also occur on land, although recent advances have been made in the recognition of impact events that occurred in the shallow marine environment. Dypvik

and Jansa [34] recognized 16 marine impact structures and bathypelagic ejecta (Eltainin, South Pacific), 6 of which are still currently in the marine environment. However, besides Eltanin that occurred in ~4700 m of water, the other marine impact sites all occurred in <500 m of water, with most at depths of <200 m [34].

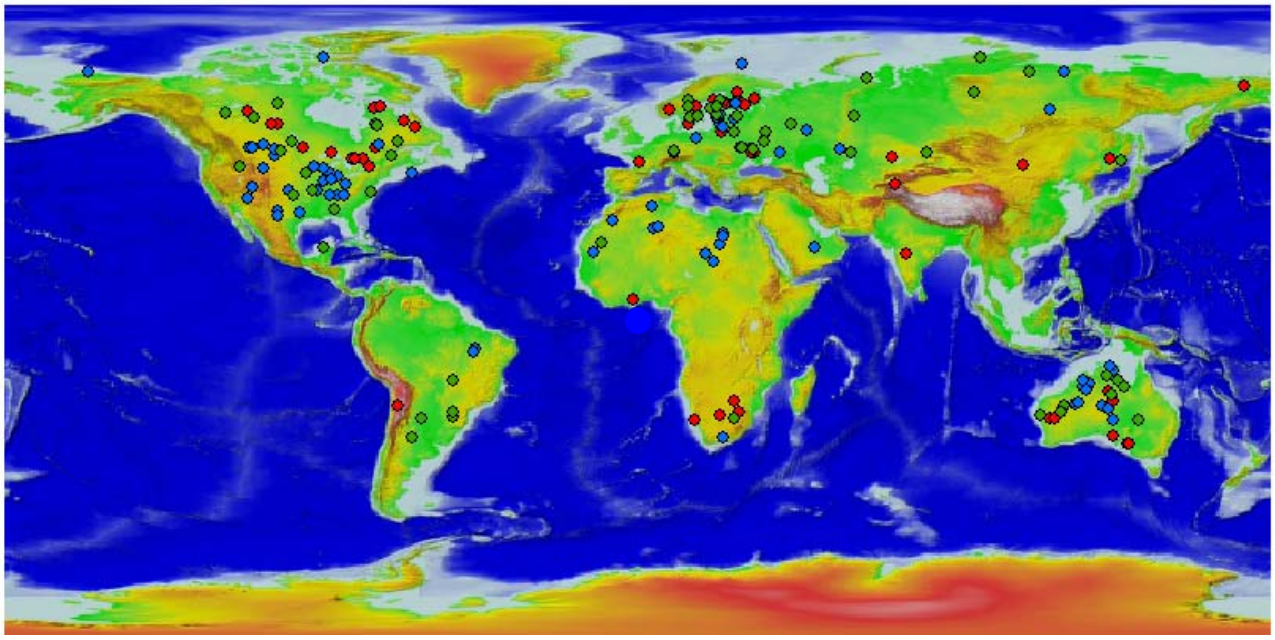

Fig. 15. Distribution of the 174 recognized terrestrial impact structures superimposed on a digital elevation map of the Earth. The red dots represent structures formed entirely in crystalline target rocks; blue dots represent structures formed entirely in sedimentary target rocks; and green dots represent mixed crystalline–sedimentary targets. Location of structures from the Earth Impact Database [2] (see Appendix 1).

6.2. Age distribution of terrestrial impact structures

There is a clear bias in the ages of terrestrial impact structures, with over half of the known structures being <200 Ma. Questions remain as to whether the cratering record has been falling off smoothly since the end of the Late Heavy Bombardment, or if there are periods of enhanced flux. Caution should be exercised given the incompleteness of the terrestrial cratering record; however, it is interesting to note the large number of Ordovician craters (Fig. 16), the majority of which are in Northern Europe [35], which also coincides with a proposed rain of ordinary chondritic meteorites [36]. The age distribution of young (<50 Ma) craters is also noticeably asymmetric (Fig. 16). In particular, there is evidence for an increased flux during the Late Eocene (Fig. 16), with several well-dated large impact craters and evidence for enhanced flux of interplanetary dust. Recent re-dating of the Haughton structure also raises the possibility of two periods of increased flux during the Eocene [37], one around 35 Ma (Popigai, Russia; Chesapeake, USA) and 39 Ma (Haughton, Wanapitei, Mistastin, Canada).

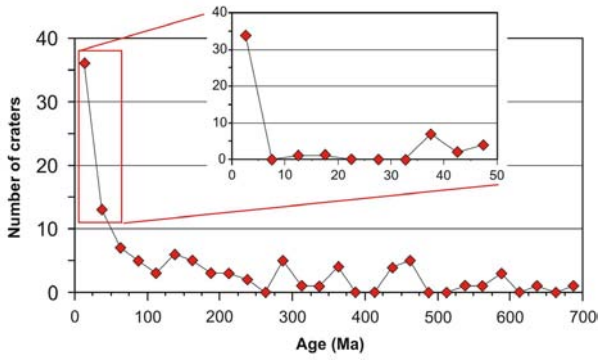

Fig. 16. Frequency plot showing known crater ages (n = 125). Note that only craters with reliable radiometric or stratigraphic ages are plotted.

7. ACKNOWLEDGEMENTS

This paper is based, in part, on Chapter 1 of the author's Ph.D. thesis. John Spray is thanked for providing and upkeeping the Earth Impact Database. This paper benefited from discussions with Richard Grieve.

8. REFERENCES

1. French, B.M., The importance of being cratered: The new role of meteorite impact as a normal geological process, *Meteoritics & Planetary Science* Vol. 39 169-197, 2004.
2. Earth Impact Database, <http://www.unb.ca/passc/ImpactDatabase/> Accessed: 25th June.2006.
3. Gault, D.E., Quaide, W.L., Oberbeck, V.R., Impact cratering mechanics and structures, in: B.M. French, N.M. Short, (Eds), *Shock Metamorphism of Natural Materials*, Mono Book Corp., Baltimore, 1968, pp. 87-99.
4. Kieffer, S.W., Simonds, C.H., The role of volatiles and lithology in the impact cratering process, *Reviews of Geophysics and Space Physics* Vol. 18 143-181, 1980.
5. Osinski, G.R., *Hypervelocity impacts into sedimentary targets: Processes and products*, PhD Thesis, University of New Brunswick, 2004.
6. Melosh, H.J., *Impact Cratering: A Geologic Process*, Oxford University Press, New York, 1989.
7. Ahrens, T.J., O'Keefe, J.D., Shock melting and vaporization of Lunar rocks and minerals, *Moon* Vol. 4 214-249, 1972.
8. Grieve, R.A.F., Dence, M.R., Robertson, P.B., Cratering processes: As interpreted from the occurrence of impact melts, in: D.J. Roddy, R.O. Pepin, R.B. Merrill, (Eds), *Impact and Explosion Cratering*, Pergamon Press, New York, 1977, pp. 791-814.
9. Graup, G., Carbonate-silicate liquid immiscibility upon impact melting: Ries Crater, Germany, *Meteoritics & Planetary Science* Vol. 34 425-438, 1999.
10. Jones, A.P., Claeys, P., Heuschkel, S., Impact melting of carbonates from the Chicxulub Crater, in: I. Gilmour, C. Koeberl, (Eds), *Impacts and the Early Earth, Lecture Notes in Earth Sciences 91*, Springer-Verlag, Berlin, 2000, pp. 343-361.
11. Osinski, G.R., Spray, J.G., Impact-generated carbonate melts: Evidence from the Haughton Structure, Canada, *Earth and Planetary Science Letters* Vol. 194 17-29, 2001.
12. Osinski, G.R., Spray, J.G., Lee, P., Impactites of the Haughton impact structure, Devon Island, Canadian High Arctic, *Meteoritics & Planetary Science* Vol. 40 1789–1812, 2005.
13. Dence, M.R., Shock zoning at Canadian Craters: Petrography and structural implications, in: B.M. French, N.M. Short, (Eds), *Shock Metamorphism of Natural Materials*, Mono Book Corp., Baltimore, 1968, pp. 169-184.
14. Grieve, R.A.F., Cintala, M.J., A method for estimating the initial impact conditions of terrestrial cratering events, exemplified by its application to Brent crater, Ontario, *Proceedings of the Lunar and Planetary Science Conference* Vol. 12B 1607-1621, 1981.
15. Stöffler, D., Gault, D.E., Wedekind, J., Polkowski, G., Experimental hypervelocity impact into quartz sand: Distribution and shock metamorphism of ejecta, *Journal of Geophysical Research* Vol. 80 4062-4077, 1975.
16. French, B.M., *Traces of Catastrophe. Handbook of Shock-Metamorphic Effects in Terrestrial Meteorite Impact Structures*, Lunar and Planetary Institute, Houston, 1998.
17. Grieve, R.A.F., Terrestrial impact structures, *Annual Review of Earth and Planetary Science* Vol. 15 245-270, 1987.
18. Melosh, H.J., Ivanov, B.A., Impact crater collapse, *Annual Review of Earth and Planetary Science* Vol. 27 385-415, 1999.
19. Dence, M.R., The extraterrestrial origin of Canadian craters, *Annals of the New York Academy of Science* Vol. 123 941-969, 1965.
20. Kenkmann, T., Ivanov, B.A., Stöffler, D., Identification of ancient impact structures: Low-angle faults and related geological features of crater basements, in: I. Gilmour, C. Koeberl, (Eds), *Impacts and the Early Earth, Lecture Notes in Earth Sciences 91*, Springer-Verlag, Berlin, 2000, pp. 279-309.
21. Newsom, H.E., Hydrothermal alteration of impact melt sheets with implications for Mars, *Icarus* Vol. 44 207-216, 1980.
22. Osinski, G.R., Lee, P., Parnell, J., Spray, J.G., Baron, M., A case study of impact-induced hydrothermal activity: The Haughton impact structure, Devon Island, Canadian High Arctic, *Meteoritics & Planetary Science* Vol. 40 1859-1878, 2005.
23. Naumov, M.V., Principal features of impact-generated hydrothermal circulation systems: mineralogical and geochemical evidence, *Geofluids* Vol. 5 165-184, 2005.
24. Turtle, E.P., Pierazzo, E., Collins, G.S., Osinski, G.R., Melosh, H.J., Morgan, J.V., Reimold, W.U., Impact structures: What does crater diameter mean? in: T. Kenkmann, F. Hörz, A. Deutsch, (Eds), *Large meteorite impacts III: Geological Society of America Special Paper 384*, Geological Society of America, Boulder, 2005, pp. 1-24.
25. Dence, M.R., The nature and significance of terrestrial impact structures, *International Geological Congress Proceedings* Vol. 24th 77-89, 1972.
26. Milton, D.J., Macdonald, F.A., Goat Paddock, Western Australia: an impact crater near the simplecomplex transition, *Australian Journal of Earth Sciences* Vol. 52 689-697, 2005.
27. Stewart, S.A., Allen, P.J., A 20-km-diameter multi-ringed impact structure in the North Sea, *Nature* Vol. 418 520-523, 2002.

28. Underhill, J.R., Earth science An alternative origin for the "Silverpit crater", *Nature* Vol. 428 doi: 10.1038/nature02476, 2004.
29. Stewart, S.A., How will we recognize buried impact craters in terrestrial sedimentary basins? *Geology* Vol. 31 929-932, 2003.
30. Barringer, D.M., *Proc. Acad. Natl. Sci. Philos.* Vol. 66 861-886, 1905.
31. Puura, V., Plado, J., Settings of meteorite impact structures in the Svecofennia crustal domain, in: C. Koeberl, H. Henkel, (Eds), *Impact Tectonics*, Impact Studies Series, Volume 6, Springer-Verlag, Berlin, 2005, pp. 211-245.
32. Haines, P.W., Impact cratering and distal ejecta: the Australian record, *Australian Journal of Earth Sciences* Vol. 52 481-507, 2005.
33. French, B.M., Short, N.M., *Shock Metamorphism of Natural Materials*, Mono Book Corp., Baltimore, 1968.
34. Dypvik, H., Jansa, L.F., Sedimentary signatures and processes during marine bolide impacts: a review, *Sedimentary Geology* Vol. 161 309-337, 2003.
35. Lindström, M., Puura, V., Floden, T., Bruun, A., Ordovician impacts at sea in Baltoscandia, *International Conference on Large Meteorite Impacts and Planetary Evolution*, Lunar and Plantary Institute, 1992, p. 47.
36. Schmitz, B., Tassinari, M., Peucker-Ehrenbrink, B., A rain of ordinary chondritic meteorites in the early Ordovician, *Earth and Planetary Science Letters* Vol. 194 1-15, 2001.
37. Sherlock, S.C., Kelley, S.P., Parnell, J., Green, P., Lee, P., Osinski, G.R., Cockell, C.S., Re-evaluating the age of Haughton impact event, *Meteoritics & Planetary Science* Vol. 40 1777-1787, 2005.

Appendix 1. List of confirmed terrestrial impact structures with their important attributes (data from the Earth Impact Database, 2006) and a summary of the target stratigraphy (this study).

Crater name	Location	Latitude	Longitude	Age (Ma)	Diameter (km)	Target rock[1]
Acraman	Australia	S 32° 1'	E 135° 27'	~590	90	C
Ames	U.S.A.	N 36° 15'	W 98° 12'	470 ± 30	16	M
Amelia Creek	Australia	S 20° 55'	E 134 ° 50'	1640– 600	~20	M
Amguid	Algeria	N 26° 5'	E 4° 23'	< 0.1	0.45	S
Aorounga	Chad	N 19° 6'	E 19° 15'	< 345	12.6	S
Aouelloul	Mauritania	N 20° 15'	W 12° 41'	3.0 ± 0.3	0.39	S
Araguainha	Brazil	S 16° 47'	W 52° 59'	244.40 ± 3.25	40	M
Arkenu 1	Libya	N 22° 4'	E 23° 45'	< 140	6.8	S
Arkenu 2	Libya	N 22° 4'	E 23° 45'	< 140	10	S
Avak	U.S.A.	N 71° 15'	W 156° 38'	3-95	12	S
B.P. Structure	Libya	N 25° 19'	E 24° 20'	< 120	2	S
Barringer	U.S.A.	N 35° 2'	W 111° 1'	0.049 ± 0.003	1.186	S
Beaverhead	U.S.A.	N 44° 36'	W 113° 0'	~ 600	60	M
Beyenchime-Salaatin	Russia	N 71° 0'	E 121° 40'	40 ± 20	8	S
Bigach	Kazakhstan	N 48° 34'	E 82° 1'	5 ± 3	8	M
Boltysh	Ukraine	N 48° 45'	E 32° 10'	65.17 ± 0.64	24	C
Bosumtwi	Ghana	N 6° 30'	W 1° 25'	1.07	10.5	C-Ms
Boxhole	Australia	S 22° 37'	E 135° 12'	0.0540 ± 0.0015	0.17	C
Brent	Canada	N 46° 5'	W 78° 29'	396 ± 20	3.8	C
Calvin	USA	N 41° 50'	W 85° 57'	450 ± 10	8.5	S
Campo Del Cielo	Argentina	S 27° 38'	W 61° 42'	< 0.004	0.05	M
Carswell	Canada	N 58° 27'	W 109° 30'	115 ± 10	39	M
Charlevoix	Canada	N 47° 32'	W 70° 18'	342 ± 15	54	M
Chesapeake Bay	U.S.A.	N 37° 17'	W 76° 1'	35.5 ± 0.3	90	M
Chicxulub	Mexico	N 21° 20'	W 89° 30'	64.98 ± 0.05	170	M
Chiyli	Kazakhstan	N 49° 10'	E 57° 51'	46 ± 7	5.5	S
Chukcha	Russia	N 75° 42'	E 97° 48'	< 70	6	M
Clearwater East	Canada	N 56° 5'	W 74° 7'	290 ± 20	26	M
Clearwater West	Canada	N 56° 13'	W 74° 30'	290 ± 20	36	M
Cloud Creek	U.S.A.	N 43° 7'	W 106° 45'	190 ± 30 Ma	7	S
Connolly Basin	Australia	S 23° 32'	E 124° 45'	< 60	9	S

Crater name	Location	Latitude	Longitude	Age (Ma)	Diameter (km)	Target rock[1]
Couture	Canada	N 60° 8'	W 75° 20'	430 ± 25	8	C
Crawford	Australia	S 34° 43'	E 139° 2'	> 35	8.5	C-Ms
Crooked Creek	U.S.A.	N 37° 50'	W 91° 23'	320 ± 80	7	S
Dalgaranga	Australia	S 27° 38'	E 117° 17'	~ 0.27	0.024	C
Decaturville	U.S.A.	N 37° 54'	W 92° 43'	< 300	6	M
Deep Bay	Canada	N 56° 24'	W 102° 59'	99 ± 4	13	C
Dellen	Sweden	N 61° 48'	E 16° 48'	89.0 ± 2.7	19	C
Des Plaines	U.S.A.	N 42° 3'	W 87° 52'	< 280	8	S
Dobele	Latvia	N 56° 35'	E 23° 15'	290 ± 35	4.5	S
Eagle Butte	Canada	N 49° 42'	W 110° 30'	< 65	10	S
Elbow	Canada	N 50° 59'	W 106° 43'	395 ± 25	8	S
El'gygytgyn	Russia	N 67° 30'	E 172° 5'	3.5 ± 0.5	18	C
Flaxman	Australia	S 34° 37'	E 139° 4'	> 35	10	C-Ms
Flynn Creek	U.S.A.	N 36° 17'	W 85° 40'	360 ± 20	3.8	S
Foelsche	Australia	S 16° 40'	E 136° 47'	> 545	6	M
Gardnos	Norway	N 60° 39'	E 9° 0'	500 ± 10	5	C
Glasford	U.S.A.	N 40° 36'	W 89° 47'	< 430	4	S
Glikson	Australia	S 23° 59'	E 121° 34'	< 508	~19	M
Glover Bluff	U.S.A.	N 43° 58'	W 89° 32'	< 500	8	S
Goat Paddock	Australia	S 18° 20'	E 126° 40'	< 50	5.1	S
Gosses Bluff	Australia	S 23° 49'	E 132° 19'	142.5 ± 0.8	22	S
Gow	Canada	N 56° 27'	W 104° 29'	< 250	5	C
Goyder	Australia	S 13° 9'	E 135° 2'	< 1400	3	S
Granby	Sweden	N 58° 25'	E 14° 56'	~ 470	3	M
Gusev	Russia	N 48° 26'	E 40° 32'	49.0 ± 0.2	3	S
Gweni-Fada	Africa	N 17° 25'	E 21° 45'	< 345	14	S
Haughton	Canada	N 75° 22'	W 89° 41'	39 ± 2	23	S
Haviland	U.S.A.	N 37° 35'	W 99° 10'	< 0.001	0.015	S
Henbury	Australia	S 24° 34'	E 133° 8'	.0042 ± 0.0019	0.157	S
Holleford	Canada	N 44° 28'	W 76° 38'	550 ± 100	2.35	C
Ile Rouleau	Canada	N 50° 41'	W 73° 53'	< 300	4	S
Ilumetsä	Estonia	N 57° 58'	E 27° 25'	> 0.002	0.08	S
Ilyinets	Ukraine	N 49° 7'	E 29° 6'	378 ± 5	8.5	M
Iso-Naakkima	Finland	N 62° 11'	E 27° 9'	> 1000	3	S
Jänisjärvi	Russia	N 61° 58'	E 30° 55'	700 ± 5	14	C-Ms
Kaalijärv	Estonia	N 58° 24'	E 22° 40'	0.004 ± 0.001	0.11	S
Kalkkop	South Africa	S 32° 43'	E 24° 34'	< 1.8	0.64	S
Kaluga	Russia	N 54° 30'	E 36° 12'	380 ± 5	15	M
Kamensk	Russia	N 48° 21'	E 40° 30'	49.0 ± 0.2	25	S
Kara	Russia	N 69° 6'	E 64° 9'	70.3 ± 2.2	65	M
Kara-Kul	Tajikistan	N 39° 1'	E 73° 27'	< 5	52	C
Kärdla	Estonia	N 59° 1'	E 22° 46'	~ 455	4	M
Karikkoselkä	Finland	N 62° 13'	E 25° 15'	< 1.88	1.5	C
Karla	Russia	N 54° 55'	E 48° 2'	5 ± 1	10	S
Kelly West	Australia	S 19° 56'	E 133° 57'	> 550	10	C-Ms
Kentland	U.S.A.	N 40° 45'	W 87° 24'	< 97	13	S
Keurusselkä	Finland	N 62° 8'	E 24° 36'	<1800	30	C
Kgagodi	Botswana	S 22° 29'	E 27° 35'	< 180	3.5	C
Kursk	Russia	N 51° 42'	E 36° 0'	250 ± 80	6	M
La Moinerie	Canada	N 57° 26'	W 66° 37'	400 ± 50	8	C
Lappajärvi	Finland	N 63° 12'	E 23° 42'	73.3 ± 5.3	23	M
Lawn Hill	Australia	S 18° 40'	E 138° 39'	> 515	18	M
Liverpool	Australia	S 12° 24'	E 134° 3'	150 ± 70	1.6	S
Lockne	Sweden	N 63° 0'	E 14° 49'	455	7.5	M
Logancha	Russia	N 65° 31'	E 95° 56'	40 ± 20	20	M
Logoisk	Belarus	N 54° 12'	E 27° 48'	42.3 ± 1.1	15	M

Crater name	Location	Latitude	Longitude	Age (Ma)	Diameter (km)	Target rock[1]
Lonar	India	N 19° 58'	E 76° 31'	0.052 ± 0.006	1.83	C
Lumparn	Finland	N 60° 9'	E 20° 6'	~ 1000	9	M
Macha	Russia	N 60° 6'	E 117° 35'	< 0.007	0.3	S
Manicouagan	Canada	N 51° 23'	W 68° 42'	214 ± 1	100	M
Manson	Iowa, U.S.A.	N 42° 35'	W 94° 33'	73.8 ± 0.3	35	M
Maple Creek	Canada	N 49° 48'	W 109° 6'	< 75	6	S
Marquez	U.S.A.	N 31° 17'	W 96° 18'	58 ± 2	12.7	S
Middlesboro	U.S.A.	N 36° 37'	W 83° 44'	< 300	6	S
Mien	Sweden	N 56° 25'	E 14° 52'	121.0 ± 2.3	9	C
Mishina Gora	Russia	N 58° 43'	E 28° 3'	300 ± 50	4	M
Mistastin	Canada	N 55° 53'	W 63° 18'	36.4 ± 4	28	C
Mizarai	Lithuania	N 54° 1'	E 23° 54'	500 ± 20	5	C
Mjølnir	Norway	N 73° 48'	E 29° 40'	142.0 ± 2.6	40	S
Montagnais	Canada	N 42° 53'	W 64° 13'	50.50 ± 0.76	45	S
Monturaqui	Chile	S 23° 56'	W 68° 17'	< 1	0.46	C
Morasko	Poland	N 52° 29'	E 16° 54'	< 0.01	0.1	S
Morokweng	South Africa	S 26° 28'	E 23° 32'	145.0 ± 0.8	70	C
Mount Toondina	South Australia	S 27° 57'	E 135° 22'	< 110	4	S
Neugrund	Estonia	N 59° 20'	E 23° 40'	~ 470	8	S
New Quebec	Canada	N 61° 17'	W 73° 40'	1.4 ± 0.1	3.44	C
Newporte	U.S.A.	N 48° 58'	W 101° 58'	< 500	3.2	M
Nicholson	Canada	N 62° 40'	W 102° 41'	< 400	12.5	M
Oasis	Libya	N 24° 35'	E 24° 24'	< 120	18	S
Obolon	Ukraine	N 49° 35'	E 32° 55'	169 ± 7	20	M
Odessa	U.S.A.	N 31° 45'	W 102° 29'	< 0.05	0.168	S
Ouarkziz	Algeria	N 29° 0'	W 7° 33'	< 70	3.5	S
Paasselkä	Finland	N 62° 2'	E 29° 5'	< 1800	10	
Piccaninny	Australia	S 17° 32'	E 128° 25'	< 360	7	S
Pilot	Canada	N 60° 17'	W 111° 1'	445 ± 2	6	C
Popigai	Russia	N 71° 39'	E 111° 11'	35.7 ± 0.2	100	M
Presqu'ile	Canada	N 49° 43'	W 74° 48'	< 500	24	C
Puchezh-Katunki	Russia	N 56° 58'	E 43° 43'	167 ± 3	80	M
Ragozinka	Russia	N 58° 44'	E 61° 48'	46 ± 3	9	M
Red Wing	U.S.A.	N 47° 36'	W 103° 33'	200 ± 25	9	S
Riachao Ring	Brazil	S 7° 43'	W 46° 39'	< 200	4.5	S
Ries	Germany	N 48° 53'	E 10° 37'	15.1 ± 0.1	24	M
Rio Cuarto	Argentina	S 32° 52'	W 64° 14'	< 0.1	1 by 4.5	M
Rochechouart	France	N 45° 50'	E 0° 56'	214 ± 8	23	C
Rock Elm	U.S.A.	N 44° 43'	W 92° 14'	< 505	6	S
Roter Kamm	Namibia	S 27° 46'	E 16° 18'	3.7 ± 0.3	2.5	C
Rotmistrovka	Ukraine	N 49° 0'	E 32° 0'	120 ± 10	2.7	C
Sääksjärvi	Finland	N 61° 24'	E 22° 24'	~ 560	6	M
Saarijärvi	Finland	N 65° 17'	E 28° 23'	> 600	1.5	C
Saint Martin	Canada	N 51° 47'	W 98° 32'	220 ± 32	40	M
Serpent Mound	Ohio, U.S.A.	N 39° 2'	W 83° 24'	< 320	8	S
Serra da Cangalha	Brazil	S 8° 5'	W 46° 52'	< 300	12	S
Shoemaker (formerly Teague Ring)	Australia	S 25° 52'	E 120° 53'	1630 ± 5	30	M
Shunak	Kazakhstan	N 47° 12'	E 72° 42'	45 ± 10	2.8	C
Sierra Madera	U.S.A.	N 30° 36'	W 102° 55'	< 100	13	S
Sikhote Alin	Russia	N 46° 7'	E 134° 40'	0.000055	0.027	C
Siljan	Sweden	N 61° 2'	E 14° 52'	361.0 ± 1.1	52	M
Slate Islands	Canada	N 48° 40'	W 87° 0'	~ 450	30	C
Sobolev	Russia	N 46° 18'	E 137° 52'	< 0.001	0.053	M

Crater name	Location	Latitude	Longitude	Age (Ma)	Diameter (km)	Target rock[1]
Söderfjärden	Finland	N 63° 2'	E 21° 35'	~ 600	5.5	C
Spider	Australia	S 16° 44'	E 126° 5'	> 570	13	S
Steen River	Canada	N 59° 30'	W 117° 38'	91± 7	25	M
Steinheim	Germany	N 48° 41'	E 10° 4'	15 ± 1	3.8	S
Strangways	Australia	S 15° 12'	E 133° 35'	646 ± 42	25	M
Suavjärvi	Russia	N 63° 7'	E 33° 23'	~ 2400	16	C-Ms
Sudbury	Canada	N 46° 36'	W 81° 11'	1850 ± 3	250	C
Suvasvesi N	Finland	N 62° 42'	E 28° 10'	< 1000	4	C
Tabun-Khara-Obo	Mongolia	N 44° 6'	E 109° 36'	150 ± 20	1.3	C
Talemzane	Algeria	N 33° 19'	E 4° 2'	< 3	1.75	S
Tenoumer	Mauritania	N 22° 55'	W 10° 24'	0.0214 ± 0.0097	1.9	M
Ternovka	Ukraine	N 48° 08'	E 33° 31'	280 ± 10	11	C
Tin Bider	Algeria	N 27° 36'	E 5° 7'	< 70	6	S
Tookoonooka	Australia	S 27° 7'	E 142° 50'	128 ± 5	55	M
Tswaing (formerly Pretoria Saltpan)	South Africa	S 25° 24'	E 28° 5'	0.220 ± 0.052	1.13	C
Tvären	Sweden	N 58° 46'	E 17° 25'	~ 455	2	M
Upheaval Dome	U.S.A.	N 38° 26'	W 109° 54'	< 170	10	S
Vargeao Dome	Brazil	S 26° 50'	W 52° 7'	< 70	12	M
Veevers	Australia	S 22° 58'	E 125° 22'	< 1	0.08	S
Vepriai	Lithuania	N 55° 5'	E 24° 35'	> 160 ± 10	8	S
Viewfield	Canada	N 49° 35'	W 103° 4'	190 ± 20	2.5	S
Vista Alegre	Brazil	S 25° 57'	W 52° 41'	< 65	9.5	
Vredefort	South Africa	S 27° 0'	E 27° 30'	2023 ± 4	300	M
Wabar	Saudi Arabia	N 21° 30'	E 50° 28'	0.00014	0.116	S
Wanapitei	Canada	N 46° 45'	W 80° 45'	37.2 ± 1.2	7.5	C
Wells Creek	U.S.A.	N 36° 23'	W 87° 40'	200 ± 100	12	S
West Hawk	Canada	N 49° 46'	W 95° 11'	351± 20	2.44	C
Wetumpka	U.S.A.	N 32° 31'	W 86° 10'	81.0 ± 1.5	6.5	M
Wolfe Creek	Australia	S 19° 10'	E 127° 48'	< 0.3	0.875	S
Woodleigh	Australia	S 26° 3'	E 114° 39'	364 ± 8	40	M
Yarrabubba	Australia	S 27° 10'	E 118° 50'	~ 2000	30	C
Zapadnaya	Ukraine	N 49° 44'	E 29° 0'	165 ± 5	3.2	C
Zelenv Gai	Ukraine	N 48° 4'	E 32° 45'	80 ± 20	2.5	C
Zhamanshin	Kazakhstan	N 48° 24'	E 60° 58'	0.9 ± 0.1	14	M

[1]Abbreviations: C = crystalline target; C-Ms = metasedimentary target; M = mixed target (i.e., sedimentary strata overlying crystalline basement); S = sedimentary target (i.e., no crystalline rocks affected by the impact event);